Dissociative electron attachment to C2F5 radicals

Dissociative electron attachment to C2F5 radicals

Sean A. Haughey, Thomas A. Field, Judith Langer, Nicholas S. Shuman, Thomas M. Miller et al.

Citation: J. Chem. Phys. **137**, 054310 (2012); doi: 10.1063/1.4738759
View online: http://dx.doi.org/10.1063/1.4738759
View Table of Contents: http://jcp.aip.org/resource/1/JCPSA6/v137/i5
Published by the American Institute of Physics.

Dissociative electron attachment to C_2F_5 radicals

Sean A. Haughey,[1] Thomas A. Field,[1,a)] Judith Langer,[2] Nicholas S. Shuman,[3] Thomas M. Miller,[3] Jeffrey F. Friedman,[3] and A. A. Viggiano[3]
[1]*Centre for Plasma Physics, School of Mathematics and Physics, Queen's University Belfast, Belfast BT7 1NN, United Kingdom*
[2]*Technische Universitaet Berlin, Institut Optik und Atomare Physik, Hardenbergstr. 36, 10623 Berlin, Germany*
[3]*Air Force Research Laboratory, Space Vehicles Directorate, Kirtland Air Force Base, New Mexico 87117-5776, USA*

(Received 29 May 2012; accepted 9 July 2012; published online 3 August 2012)

Dissociative electron attachment to the reactive C_2F_5 molecular radical has been investigated with two complimentary experimental methods; a single collision beam experiment and a new flowing afterglow Langmuir probe technique. The beam results show that F^- is formed close to zero electron energy in dissociative electron attachment to C_2F_5. The afterglow measurements also show that F^- is formed in collisions between electrons and C_2F_5 molecules with rate constants of 3.7×10^{-9} cm^3 s^{-1} to 4.7×10^{-9} cm^3 s^{-1} at temperatures of 300–600 K. The rate constant increases slowly with increasing temperature, but the rise observed is smaller than the experimental uncertainty of 35%. [http://dx.doi.org/10.1063/1.4738759]

I. INTRODUCTION

Low temperature technological fluorocarbon plasmas are used widely in industry, for example, to etch silicon dioxide in semiconductor processing and to deposit hydrophobic polymeric fluorocarbon layers. Such technological plasmas are, of course, chemically potent as they contain free electrons, positively and negatively charged ions, atoms, radicals, and excited states. The dynamics and chemistry of plasmas are complex. It has been stated that the main roadblock in the development of plasma models is a lack of fundamental data for the atomic and molecular processes that occur in plasmas.[1] In particular, data for radicals, reactive molecules and excited states have been highlighted as a particular area of need. These species are critical to the overall chemical and physical processes occurring in the plasma, but on the other hand they are so reactive that for experimental investigations they generally need to be generated *in situ* and gas samples may be impure.

Collisions between low energy electrons and molecules can lead to the formation of negative ions through associative electron attachment and dissociative electron attachment.[2] Both of these processes commence with the electron, e^-, becoming attached to the molecule, say AB, to form a superexcited anionic state of the molecule, AB^-*, thus

$$AB + e^- \rightarrow AB^{-*}. \quad (1)$$

The anion, AB^-*, is superexcited because when it is first formed the combined energy of the free electron and the neutral molecule is necessarily higher than the ionization energy of the anion, AB^-. Therefore, an electron can readily be lost from AB^-* in autodetachment, which can also be described as autoionization. If, however, the electron becomes attached in, for example, a shape resonance or Feshbach resonance then it may be trapped on the molecule long enough for the nuclei to move and for the molecule to dissociate by

$$AB^{-*} \rightarrow A + B^-, \quad (2)$$

where A and B^- may be atoms or multiatomic molecular fragments. This overall process of electron capture and molecular fragmentation is dissociative electron attachment. In some special cases, most famously SF_6, electrons with close to zero kinetic energy can attach to form superexcited states with lifetimes in the microsecond, millisecond or even second range.[3] It is possible to detect negatively charged parent ions, such as SF_6^- in such cases. Such close to zero energy electron attachment processes can have very large cross sections; for example, electron attachment to SF_6 has a cross section of over 1000 Å^2 at 1 meV collision energy.[4] Plasmas contain high densities of low energy free electrons and, thus, such low energy attachment processes can play a very important role in the overall behaviour of plasmas.

Laboratory investigations of electron attachment to molecules can be split into two main groups; single collision experiments and multiple collision experiments. In single collision experiments a beam of electrons with well defined energy interacts with the molecular target at low pressure. In multiple collision experiments, electrons and molecules interact together in a buffer gas and electron attachment rate constants are measured at the well defined temperature of the buffer gas, which can be varied. These two methods are complimentary and both have been used in the present investigation of electron attachment to the radical C_2F_5.

Previous investigations of electron attachment to reactive molecules and radicals include R-matrix calculations of low energy electron collisions with CF,[5,6] CF_2,[7] and CF_3.[8,9] Dissociative electron attachment to CF_2 was investigated experimentally, but no attachment was observed.[10] Elastic electron scattering from CF_2 has been observed and reported with

a)Electronic mail: t.field@qub.ac.uk.

Schwinger multichannel variational calculations.[11] Both these R-matrix[7] and Schwinger calculations[11] for CF_2 agree with another Schwinger calculation[12] in the prediction of a low energy electron attachment resonance at 1.5 eV or lower electron energy. This low energy resonance has not been observed experimentally because elastic scattering measurements have not been made a such low energies. Furthermore, a resonance at 1.5 eV or below could not be observed in dissociative electron attachment experiments[10] because the thresholds for formation of $F^- + CF$ and $CF^- + F$ are both above 1.9 eV.

In work related to the present study, electron attachment to CF_3 radicals has been investigated between 300 and 600 K with the same modified flowing afterglow Langmuir probe experiment used here.[13] In that work, formation of F^- in dissociative electron attachment was observed along with formation of CF_3^- anions in associative attachment; the ratio of these two channels depended strongly on the temperature and pressure of the gas. The temperature and pressure dependence of the measurements was fitted well with a kinetic modeling approach.[13]

II. EXPERIMENT

Electron attachment to C_2F_5 has been investigated with two complimentary experiments. At the Air Force Research Laboratory (AFRL), electron attachment has been studied with a new flowing afterglow Langmuir probe (FALP) technique that enables electron attachment to radicals to be observed in an inert bath gas at different temperatures. In Belfast, electron attachment to C_2F_5 has been investigated under single collision conditions at different electron energies in the "Electron Radical Interaction Chamber" (ERIC), which has been described previously.[14] Briefly, in ERIC a trochiodal electron monochromator (TEM) provides low energy electrons which interact with sample molecules in the source region of a small linear time-of-flight (TOF) mass spectrometer. The electron beam is pulsed; when all electrons have left the source region product ions are extracted into the drift tube of the time-of-flight mass spectrometer. The mass spectrometer potentials and extraction fields can be reversed so that either positively charged or negatively charged ions can be observed. The uncertainty in the electron energy scale is estimated to be ±0.2 eV. The electron energy resolution is ∼200 meV, measured from the full width half maximum (FWHM) of the SF_6^{-*} peak at 0 eV. The mass resolution of the mass spectrometer (FWHM M/ΔM) is typically from 100 to 200.

The sample gas enters the spectrometer, ERIC, through a glass inlet system, which includes an Evenson microwave cavity. In the present investigation, C_2F_5 was generated in the reaction of H atoms with C_2F_5I;

$$C_2F_5I + H \rightarrow HI + C_2F_5 \quad (3)$$

The H atoms were generated in a He/H_2 plasma generated by 60 to 100 W of 2.45 GHz radiation inside the Evenson cavity. The plasma region is separated by about 25 cm of glass tube from the interaction region. Downstream of the plasma and at a variable distance of 4–8 cm from the interaction region C_2F_5I was introduced to the gas flow. A similar method was used previously to prepare a sample of CF_2 through a two step reaction of CF_3I with H atoms; in the first step CF_3 was formed which rapidly reacts with a second H atom to give $CF_2 + HF$.[10]

At AFRL, a new flowing afterglow Langmuir probe (FALP) technique, dubbed variable electron and neutral density attachment mass spectrometry (VENDAMS), has recently been developed.[15] VENDAMS allows for measurements of attachment to short lived species, such as radicals, and a variety of information on ion-ion mutual neutralization kinetics.[16–19] The technique has been described in detail previously[15,17] and only the aspects important to the present experiments are described here. A primarily Ar^+/e^- plasma is formed by a microwave discharge in pure He with Ar added downstream at 4% of the He flow rate to convert He_2^+ and He metastables to Ar^+. Approximately 5% of the positive ions are He^+ and no negative ions are present except for very small impurity signals, e.g., Cl^-. In these experiments C_2F_5I was added through a neutral injector well after the plasma had been formed. The neutral is added in a known concentration of typically about 3×10^9 cm^{-3} using a mass flow meter. These concentrations are achieved by using dilute mixtures;[15] here, a 0.1% C_2F_5I in He mixture was used with flows of around 2 std. cm^3 min^{-1}. Chemistry initiated by electron attachment to C_2F_5I was allowed to proceed for 4.6 ms before the flowing gas encountered a sampling orifice to a quadrupole mass spectrometer with an analog multiplier. The entire flow tube is surrounded by resistance heaters and insulation in three zones for temperature variation. A moveable Langmuir probe is used to measure both the electron density along the flow tube axis and the plasma velocity. The latter is determined by pulsing the microwave discharge and noting the arrival time at the probe as a function of distance along the flow tube. The helium buffer density was 3.2×10^{16} cm^{-3} (1 Torr at 300 K) at all temperatures.

The primary data in a VENDAMS measurement are relative anion branching abundances present after the known reaction time as a function of the electron density at the reactant injector, $[e^-]_0$. The electron density is varied by a combination of moving the microwave discharge position, changing the fraction of the helium that enters the cavity region, while adjusting a complimentary downstream He flow in order to maintain a constant number density, and by adjusting the power of the microwave discharge. Achievable $[e^-]_0$ values range from below 1×10^8 to 5×10^{10} cm^{-3}.

At low $[e^-]_0$ the only significant chemistry that occurred after introduction of C_2F_5I was the primary electron attachment,

$$C_2F_5I + e^- \rightarrow I^- + C_2F_5. \quad (4)$$

We have measured the attachment rate constants for this reaction in the traditional manner, i.e., by monitoring the electron concentration as a function of distance down the flow tube, for $[e^-]_0$ low enough ($\leq 10^9$ cm^{-3}) that other processes are negligible.[20] Measurement of the plasma velocity provides the time scale for reaction. Reaction time profiles of the electron density were measured with and without the C_2F_5I added. The latter gave the diffusion rate, which tended to account for 10%–25% of the loss in electron density relative

to that lost to attachment. It is then straightforward to derive the rate constant for reaction (4).

Because every primary attachment produced a C_2F_5 radical, reaction (4) yielded a known concentration of C_2F_5 equal to the concentration of I^-. As $[e^-]_0$ was raised above the neutral concentration, electrons also attached to C_2F_5 to produce F^- in measurable quantities,

$$C_2F_5 + e^- \rightarrow F^- + C_2F_4. \quad (5)$$

Because both anions (I^- and F^-) are atomic, as is Ar^+, mutual neutralization did not occur to any measurable extent, and no further chemistry needs to be considered. The concentration of cations produced through charge transfer from Ar^+ are far too low to measurably deplete the anion concentrations because of the low neutral concentration.[21] The ratio of I^- to F^- is highly correlated with the ratio of the two rate constants for reactions (4) and (5).

The final piece of information needed to derive the rate constant for reaction (5) is the mass discrimination factor between F^- and I^- of the mass spectrometer. This discrimination factor was obtained by addition of NF_3 along with Ar to convert all electrons to F^- ions.[22] C_2F_5I was added downstream to convert quantitatively the F^- to I^-,

$$F^- + C_2F_5I \rightarrow I^- + C_2F_6. \quad (6)$$

Comparison of the loss of F^- signal to the gain in I^- signal as a function of the C_2F_5I flow yields the mass discrimination factor; for the current work this factor was 1.1 against I^-. In other cases, we have compared the discrimination factors determined with this method to those determined through a separate method of introducing two gases that deplete the e^- density the same amount at a fixed Langmuir probe position downstream. The two methods have given identical results within our uncertainty.[15]

III. RESULTS

A. Electron beam measurements

In Belfast, the presence of C_2F_5 radicals in the sample gas stream was confirmed by the measurement of positive ion mass spectra with varying electron energy. Figure 1 shows two-dimensional positive ion mass spectra where ion intensity is plotted as a function of ion time-of-flight on the abscissa and electron energy on the ordinate; spectra are shown with (a) the plasma off and (b) the plasma on. The positive ion mass spectra are not straightforward to interpret because $C_2F_5^+$ is observed as a fragment from the ionization of C_2F_5I as well as from ionization of C_2F_5. Figures 2(a) and 2(b) show integrated signals of $C_2F_5I^+$, $C_2F_5^+$, and HI^+ with the plasma off and on in the threshold region; these plots have been used to determine the appearance energies of these ions with the plasma on and off. The energy scale is calibrated to the ionization threshold of HI, 10.386 ± 0.001 eV.[23] From Figure 2(a) the appearance energy of $C_2F_5I^+$ is determined as 10.45 ± 0.15 eV. This energy is in agreement with previous determinations of the ionization energy of C_2F_5I; 10.67 eV,[24] 10.44 eV,[25] and 10.7 ± 0.1 eV.[26]

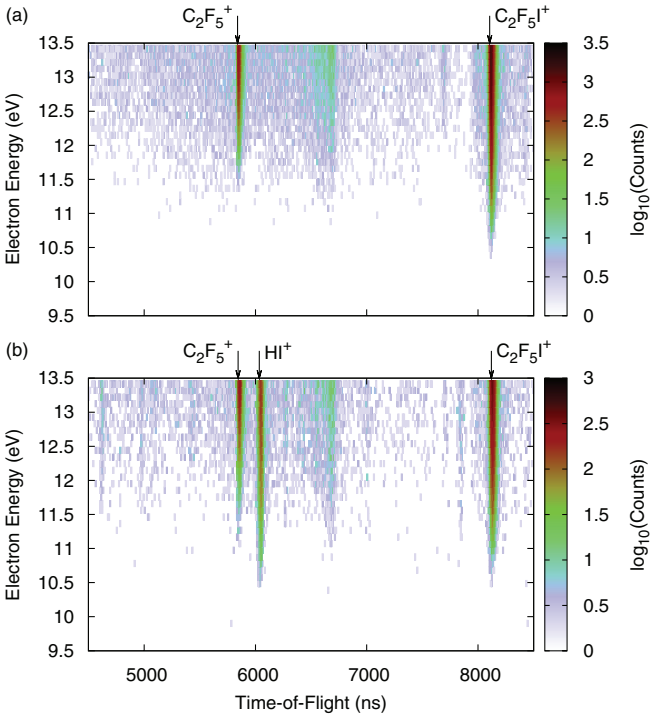

FIG. 1. Two-dimensional plots of positive ion signal as a function of time-of-flight and electron energy with (a) plasma off and (b) plasma on.

In Fig. 2(b) integrated $C_2F_5^+$ signals are shown with the plasma on and off. With the plasma off $C_2F_5^+$ is formed in dissociative ionization of C_2F_5I and an appearance energy of 11.15 ± 0.15 eV is observed here, which agrees favourably with previously determined values; 11.1 ± 0.2 eV,[25] and

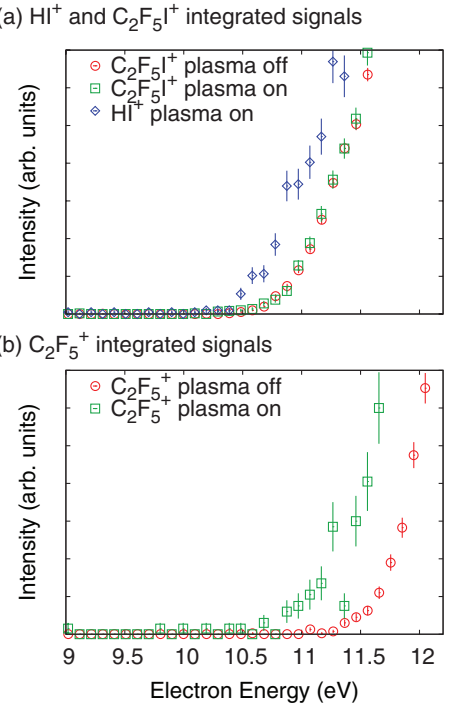

FIG. 2. Integrated positive ion signals (a) HI^+ and $C_2F_5I^+$ and (b) $C_2F_5^+$ as a function of electron energy with plasma on and off.

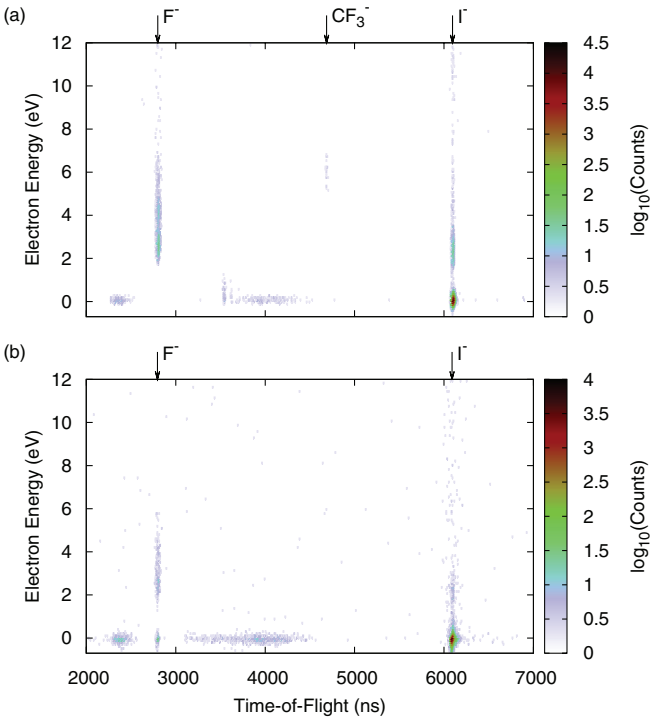

FIG. 3. Two-dimensional plots of negative ion signal as a function of time-of-flight and electron energy with (a) plasma off and (b) plasma on.

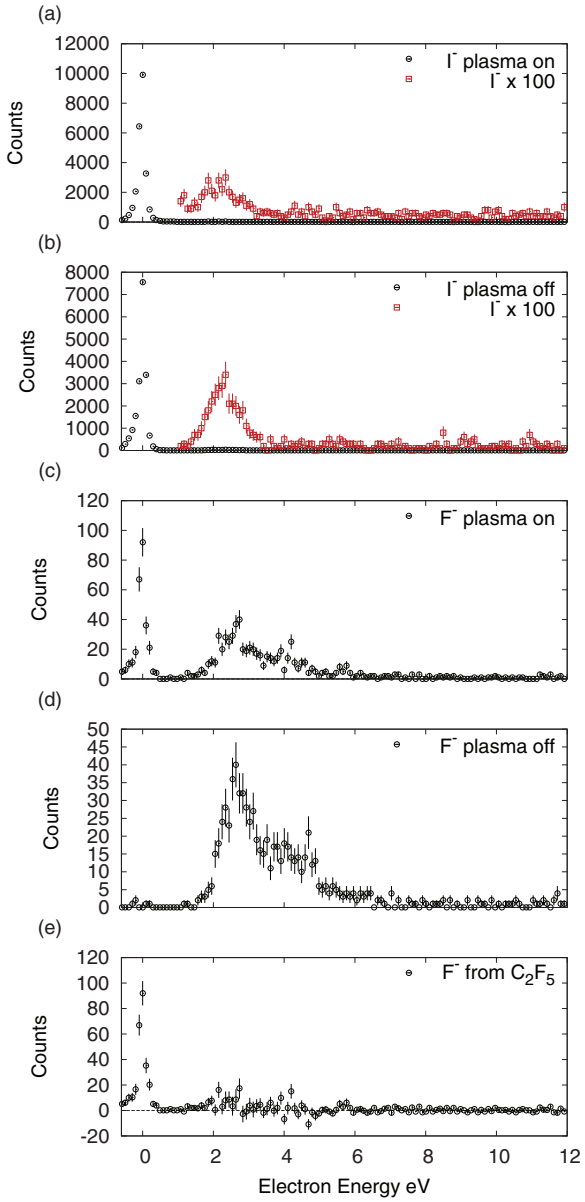

FIG. 4. Integrated I^- and F^- signals as a function of electron energy with plasma on and off. The I^- signals between 1 and 4 eV from C_2F_5I in (a) and (b) were used to determine the fraction of the F^- signal from C_2F_5I in (d) to subtract from the F^- signal with the plasma on in (c) to obtain the F^- signal from C_2F_5 shown in (e) (see text).

11.7 ± 0.1 eV.[26] The appearance energy of $C_2F_5^+$ with the plasma on observed here, 10.4 ± 0.2 eV, is significantly lower than appearance energy of $C_2F_5^+$ from C_2F_5I and close to a previously reported ionization energy for the radical C_2F_5, 9.98 eV.[27] It is concluded that the radical C_2F_5 was present in the sample gas with the plasma on. Thus, with the plasma on C_2F_5I, HI, and C_2F_5 were present in the sample gas, but only C_2F_5I was present with the plasma off.

Figure 3 shows two-dimensional spectra of negative ions formed in electron attachment with (a) the plasma off and (b) plasma on recorded under identical conditions to the positive ion spectra. An initial inspection of the data shows that in both spectra the primary negative ions formed are F^- and I^-. The clear difference between the two data sets is that with the plasma on there is a new F^- peak at 0 eV. The two spectra both have some broad noise around zero eV electron energy, which appears as a band centred at 4000 ns time-of-flight and a small island just above 2000 ns time-of-flight. This noise has been seen before in spectra of fluorine containing molecules and appears to be linked to collisions with grids in the time-of-flight mass spectrometer. There is a little background noise visible in Figure 3(b) with the plasma on across the spectrum, but note that the scale is logarithmic so the signal to noise ratio is 3 orders of magnitude or more. The noise level is lower in the spectrum with the plasma off and two faint peaks at 0 eV due to $^{35}Cl^-$ and $^{37}Cl^-$ are just visible at ∼3500 ns. There is also a very weak peak at 6 eV due to CF_3^- visible in Figure 3(a). The CF_3^- peak is not visible in Figure 3(b) because with the plasma on the number density of C_2F_5I is reduced and this signal is too weak to be seen.

Figure 4 shows integrated negative ion signals as a function of electron energy. With the plasma off only electron attachment to C_2F_5I only is observed with I^- formation at 0 eV and between 1 and 4 eV, and F^- above 1.5 eV. These results, shown in Figures 4(a) and 4(c), are in good agreement with earlier measurements of dissociative electron attachment to C_2F_5I;[28,29] the relative ion intensities agree to within ∼50%. In addition to I^- and F^- a very weak CF_3^- peak is observed at 6 eV, which was not previously observed.

With the plasma on, C_2F_5 and HI are also present in the gas stream. HI makes a contribution to the I^- signal at 0 eV in Figure 4(b), but HI does not contribute to the I^- signal between 1 and 4 eV. The F^- signal in Figure 4(d) has contributions from C_2F_5 and C_2F_5I. The contribution of C_2F_5I to the F^- signal in Figure 4(d) has been removed with the following method. First, the fraction of C_2F_5I remaining in the gas

sample with the plasma on was determined by careful comparison of the total I^- signal from C_2F_5I between 1 and 4 eV with the plasma off and on shown in Figures 4(a) and 4(b). Second, the F^- spectrum from C_2F_5I with the plasma off in Figure 4(c) was multiplied by this fraction and subtracted from the F^- spectrum taken with the plasma on, shown in Figure 4(d), to give the F^- spectrum shown in Figure 4(e) which represents the F^- ions formed in dissociative electron attachment to C_2F_5 only. No adjustable parameters were used in this subtraction procedure. It is clear that in the region between 1 and 4 eV electron energy in Figure 4(e) the F^- signal is zero after the contribution due to C_2F_5I is removed within the experimental uncertainty; the error bars shown indicate uncertainties of ±1 standard deviation and all random uncertainties have been taken into account, including the uncertainty in the fraction of C_2F_5I present with the plasma on.

The F^- spectrum due to electron attachment to C_2F_5, shown in Figure 4(e), has a strong peak at 0 eV, but has no other clear features. The uncertainty in the spectrum, however, may well hide the formation of negative ions in other dissociative electron attachment processes at higher energy, particularly between 1 and 4 eV.

B. VENDAMS data

The C_2F_5I attachment rate constant, reaction (4), was determined at each temperature in the normal FALP fashion, as described above.[20] Examples of such data are plentiful in the literature and are not shown here.[30,31] Table I shows the rate constants at various temperatures for both reactions (4) and (5) measured in the present work. Electron attachment to C_2F_5I is exothermic by 0.79 eV.[25] The rates of attachment to C_2F_5I are rapid; we estimate that it occurs in about 50% of collisions. There is a negative temperature dependence, indicative of an efficient s-wave process.[32,33] An unpublished rate constant has been referenced[25] for electron attachment to C_2F_5I of 2×10^{-8} cm^3 s^{-1} at 300 K due to Sungawa and co-workers[19,34–37] That value is incompatible with the present measurements.

Raw VENDAMS data at 500 K, corrected for mass discrimination, are shown in Figure 5. At low $[e^-]_0$, I^- is essentially the only negative ion present, with just 0.2% of the signal observed as F^-. As $[e^-]_0$ increases, the fraction of F^- increases substantially such that it is 7% of the signal at the highest density measured. Data at other temperatures are qualitatively identical. The rate constant for reaction (5), electron attachment to C_2F_5, is derived from the VENDAMS data by

TABLE I. Rate constants as a function of temperature for reactions (4) and (5).

Temperature (K)	Rate constants (cm^3 s^{-1})	
	$e^- + C_2F_5I$ (±25%)	$e^- + C_2F_5$ (±35%)
300	1.5×10^{-7}	3.7×10^{-9}
400	1.5×10^{-7}	3.8×10^{-9}
500	1.4×10^{-7}	4.4×10^{-9}
600	1.1×10^{-7}	4.5×10^{-9}

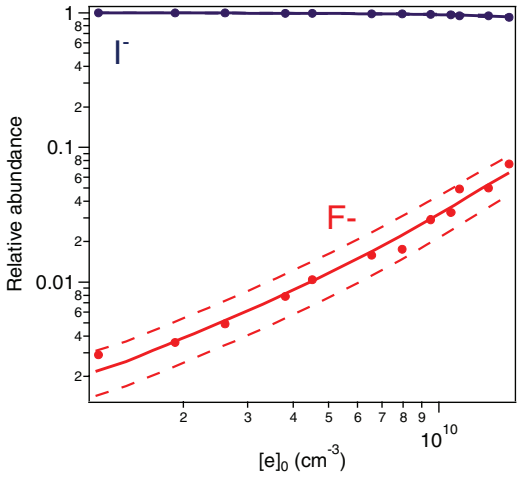

FIG. 5. VENDAMS experimental (points) and best-fit calculated (solid lines) anion abundances as a function of initial electron density 4.6 ms after addition of 3.8×10^9 cm^{-3} C_2F_5I to the afterglow at 500 K. Dashed lines are the calculated abundances at the uncertainty limits of $rmk_{C_2F_5I+e^-}$.

modeling the kinetics of all reactions occurring in the flow tube and fitting to the observed anion abundances. Experimental conditions are chosen such that only the fastest reactions amongst the species present in the highest concentrations can have any measurable effect on the anion abundances. For this study, the chemistry is extremely simple and only electron attachment to C_2F_5I and C_2F_5, reactions (4) and (5), as well as diffusion, affect the comparison of model to data. Other reactions are included in the modeling for completeness, however, ion-molecule reactions are two orders of magnitude slower than the primary attachment and do not play a role at the very low C_2F_5I densities used in VENDAMS experiments.[38] Derivation of the rate constant of reaction (5) along with uncertainty limits employs a Monte Carlo technique as follows: (1) rate constants for all reactions are randomly chosen within limits set by either a calculated collision rate or literature values where known; (2) assuming that set of rate constants, the anion abundances at the end of the 4.6 ms reaction time are calculated by iteratively solving the set of coupled differential equations describing the reaction system; (3) the calculated abundances are compared to the experimental values via a weighted least squares goodness of fit (zero being a perfect fit); (4) rate constants are varied through a simple, downhill optimization to find a local minimum in the goodness of fit; (5) the process is continuously repeated from new initial random guesses, finding other local minima until the full parameter space has been explored. For the current simple system this requires only 10^2–10^3 initial guesses and tens of seconds of computation on a desktop computer. Best fit and uncertainty limit values are determined from plots of the goodness-of-fit parameter as a function of the rate constant under consideration. Figure 6 shows a goodness-of-fit plot for the data in Figure 5 for the rate constant for electron attachment to C_2F_5, reaction (5). The solid line in Figure 5 represents the fit using the best fit value, 4.4×10^{-9} cm^3 s^{-1}; the data are reproduced extremely well. Error limits are determined by the extreme values of the rate constant at the goodness-of-fit corresponding to fits that, as

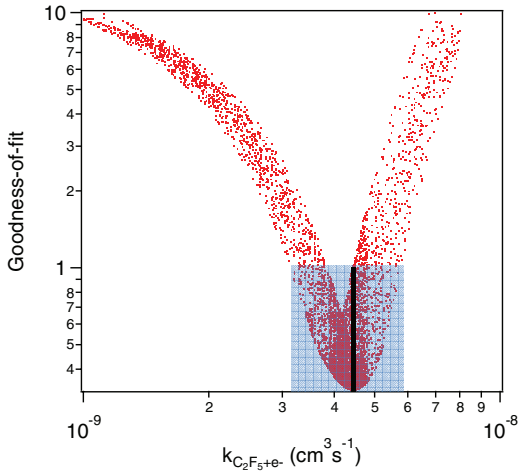

FIG. 6. Example goodness of fit plot (see text) to the data in Figure 5. The best fit value (black line) and range of acceptable fits (shaded area) from which uncertainty limits are determined are indicated.

determined by eye, clearly no longer reproduce the data. In the example shown in Figure 6 a goodness-of-fit of 1 has been chosen as the maximum allowable value. The shaded area in Figure 6 then represents acceptable fits. Error limits are determined by the extremes at a goodness-of-fit of 1 and the fits to those values are shown as dashed lines in Figure 5. The uncertainty in the C_2F_5I rate constant measurement is not fully propagated to the derivation of the C_2F_5 rate constant because the latter is largely a function of the relative, not absolute, abundances of I^- and F^-. A more in-depth description of the analysis can be found in Ref. 39.

The C_2F_5 attachment rate is almost two orders of magnitude slower than the C_2F_5I rate and increases 20% as the temperature rises from 300 to 600 K. This change, however, is well within the experimental uncertainty. The variation of rate constant with temperature can be seen in Figure 7.

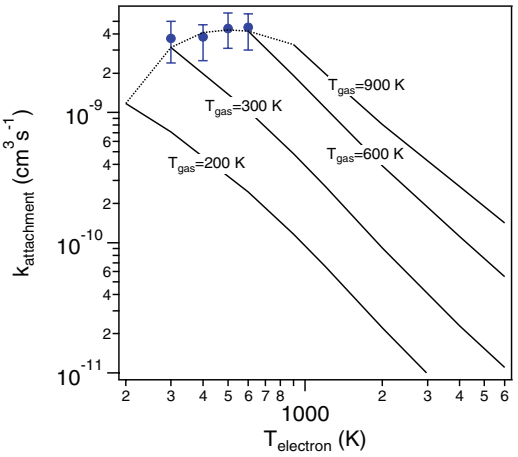

FIG. 7. Modeled rate constants (see text) of electron attachment to C_2F_5 as a function of electron temperature at the indicated gas temperatures assuming best-fit parameters (solid lines). Experimental (points) and modeled (dotted line) values corresponding to T_{gas}=$T_{electron}$ are indicated.

IV. DISCUSSION

In previous experiments in Belfast it has been possible to make an estimate of the absolute electron attachment cross section for highly reactive molecules, such as CS,[40] by making an estimate of the target molecule number density in the interaction region. Previous estimates, however, have been made at electron energies significantly above 0 eV, e.g., 4–6 eV in the case of CS. Here, however, there is an additional challenge because dissociative electron attachment to C_2F_5 occurs so close to zero energy where cross sections generally change quite dramatically over a small energy range; the experimental electron beam resolution is not sufficient to resolve the peak shape close to zero in the present work. With an electron beam resolution of ~20 μeV it has been experimentally demonstrated for SF_6 that from <10 μeV to ~10 meV the s-wave electron attachment cross section, σ, follows the theoretically predicted $\sigma \propto E^{-1/2}$ form.[41] Thus, s-wave attachment cross sections rise as the energy decreases to theoretically infinite values at zero energy. By contrast, it has also been observed experimentally, in dissociative electron attachment to Cl_2, that from ~1 to 50 meV the p-wave attachment cross section follows the theoretically predicted $\sigma \propto E^{1/2}$ form.[42] Thus, p-wave attachment cross sections drop to zero at zero energy. Therefore, it has not been possible with the electron beam data to estimate an absolute cross section for electron attachment to C_2F_5, but it has been possible with the VENDAMS data to determine rate constants at different temperatures.

Electron attachment in the multiple collision conditions of the FALP experiment can be viewed as a series of these fundamental processes:

$$C_2F_5 + e^- \xrightarrow{k_{at}} C_2F_5^{-*} \tag{7}$$

$$C_2F_5^{-*} \xrightarrow{k_{det}} C_2F_5 + e^- \tag{8}$$

$$C_2F_5^{-*} + M \xrightarrow{k_{stab}} C_2F_5^- + M \tag{9}$$

$$C_2F_5^{-*} \xrightarrow{k_{dis}} C_2F_4 + F^- \tag{10}$$

After electron capture, process (7), the excess energy of the superexcited $C_2F_5{}^-$* anion must be disposed of through one of the competing processes (8)–(10). The measured rate constants of dissociative electron attachment to C_2F_5, reaction (5), are fairly slow; only about 1 in 100 collisions results in dissociative electron attachment.[32] These rate constants depend, of course, on the rates of the individual processes (7)–(10). The collisional stabilization process, (9), can be discounted in the present case as no trace of stable parent ion $C_2F_5^-$ was observed in the VENDAMS experiment. Therefore, there are two extreme cases that can explain why only 1 in 100 collisions leads to dissociative electron attachment. In the first scenario the electron attachment is rapid and occurs at the collisional rate, but the rate of electron detachment, process (8), is ~100 times faster than dissociation, process (10). The other extreme situation would be where the rate of electron attachment is ~100 times slower than the collisional rate, but dissociation, process (10), is significantly greater than the

rate of detachment, process (8). Alternatively, there might be a situation somewhere between these two extremes.

Recently, a new method of kinetic modeling for analyzing thermal electron attachment systems has been developed by Troe and co-workers.[35–37] This method requires fitting several adjustable parameters to the data. By assuming that attachment leads to formation of a vibrationally excited $C_2F_5^{-*}$ anion in its electronic ground state, the kinetic modeling can be applied here. Briefly, collision rate constants are calculated using extended Vogt-Wannier theory.[32,33] Both the attachment rate constant (7) and the resulting energy distribution of $C_2F_5^{-*}$ are calculated using an empirical factor to account for inefficiency of capturing higher energy electrons beyond the limit set by extended Vogt-Wannier theory. This increased inefficiency may be due either to the rate of intramolecular vibrational energy redistribution i.e., the incorporation of the electron and its energy into the molecule via electron-phonon coupling) or from competition by electron scattering. Autodetachment (8) and dissociation (10) specific rate curves are calculated using statistical theory by employing microscopic reversibility[43] of (7) and by employing the simplified statistical adiabatic channel model.[44,45] Finally, competition between (8)–(10) is determined by explicitly accounting for collisions with the buffer gas and approximating the solution to the Master Equation using the many-shots approach.[13,46]

As determined with the kinetic modeling, neither stabilization of $C_2F_5^{-*}$ through collisions with the buffer gas, process (9), nor autodetachment (8) occur quickly enough to compete with the dissociation, process (10). The failure of (9) to compete is consistent with no parent anion signal being observed and not surprising as dissociative electron attachment is exothermic by 0.5 eV, as calculated with GAUSSIAN-3 (G3) theory.[47] The calculated unimolecular rate constant for autodetachment is on the order of 100 s^{-1} at threshold, while that of dissociation is, even under generous assumptions, $>10^7$ s^{-1} at the same energy. The rate of autodetachment increases more rapidly with energy, but reaches only $\sim 10^4$ s^{-1} at 0.4 eV above threshold, at which point the thermal distribution is negligible. Because autodetachment never competes effectively with dissociation, the low attachment rate constants must be due to the second extreme case presented above where the rate of electron attachment (7) occurs at only 1/100th of the maximum value.

Many thermal electron attachment processes show Arrhenius behaviour over moderate temperature ranges.[48] The C_2F_5 data may be fitted to an Arrhenius equation assuming a small activation energy of 90 cm^{-1}; corresponding to an energetic barrier between the neutral and anion potential energy surfaces where some amount of vibrational excitation is needed to surmount the barrier. The Arrhenius description tends to fail at higher energies and offers limited physical insight into the magnitude of the rate constants. Invoking the kinetic modeling approach instead, the C_2F_5 data are well fit between 300 K and 600 K by assuming purely s-wave attachment, a somewhat larger barrier of 560 ± 200 cm^{-1}, and a significant decrease in capture efficiency of higher energy electrons from that calculated using Vogt-Wannier theory. In the language of the kinetic model, $c_1 = 20$ assuming the electron capture probability as a function of collision energy falls as $e^{-c_1\kappa^2}$, where κ is proportional to the square root of the collision energy. The best fit c_1 value corresponds to a FWHM of the zero-energy peak in Figure 4(e) of 0.015 eV, much less than the upper limit of 0.2 eV set by the experimental resolution of the beam measurements; the 0.2 eV FWHM sets a lower limit on c_1 of 4. The modeling suggests a larger barrier than does an Arrhenius fit; interestingly, application of R-matrix theory to other exothermic dissociative electron attachments also suggests that Arrhenius underestimates the barrier height in such systems.[48]

The near flat temperature dependence of the rate constant over the measured range is the result of the positive dependence on the C_2F_5 internal energy distribution being offset by the negative dependence on the electron temperature. At lower temperatures, the former will dominate, and Arrhenius fit behaviour is predicted. At higher temperatures or for non-thermal plasmas, the latter will dominate and, in the absence any higher energy resonances as indicated by the beam measurements, a steep negative temperature dependence is predicted. Extrapolated attachment rate constants derived from the kinetic modeling are shown in Figure 7. Uncertainty in the extrapolated values increases at conditions far from the experiment to up to an order of magnitude; however, the qualitative trends shown may be considered robust. The temperature dependence is very similar to that of attachment to CF_3.[13] Although not measured, it is expected that due to the rapid dissociation rate of $C_2F_5^{-*}$ that the electron attachment rate constant will not have any pressure dependence even up to atmospheric pressures, which is very different to CF_3, where non-dissociative attachment occurs and there is a measurable positive pressure dependence at pressures on the order of 1 Torr. This difference stems primarily from the fact that dissociative attachment to CF_3 is slightly endothermic, while dissociative attachment to C_2F_5 is exothermic.

The observation of an anion peak close to zero electron energy is due in some cases to dissociative electron attachment to vibrationally excited molecules, rather than to molecules in the ground vibrational state. Electron attachment to vibrationally excited SF_6 molecules, for example, can lead to the observation of a peak close to zero electron energy of SF_5^- fragment ions, which is not observed in electron attachment to ground state SF_6 molecules.[49] The flat temperature dependence of the F^- formation rate constant indicates that there is no such dramatic dependence on the initial vibrational state in dissociative electron attachment to C_2F_5.

V. CONCLUSIONS

In this work the observation formation of F^- in dissociative electron attachment to C_2F_5 close to zero eV electron energy has been observed independently in two different experiments; a single collision beam experiment in Belfast and a multiple collision experiment with a buffer gas at AFRL. It has not been possible to measure absolute cross sections with the beam experiment, but the rate constant of electron attachment to C_2F_5 has been measured at AFRL. The rate constant appears to increase slightly as the temperature is raised. Rate constants measured correspond to $\sim$1 dissociative electron

attachment event per 100 collisions, which appears to be due to inefficient capture of low energy electrons by C_2F_5.

ACKNOWLEDGMENTS

The AFRL authors are grateful for the support of the Air Force Office of Scientific Research for this work. N.S.S. was supported by the National Research Council Research Associateship Program under Project No. AFOSR-2303EP. T.M.M. and J.F.F. are under contract to the Institute for Scientific Research of Boston College. The Belfast authors are grateful for the support of the EPSRC, Royal Society, and COST Action CM0601 ECCL. J.L. is grateful for Transnational Access granted by the European Project ITS LEIF (RII3-026015). Finally, many thanks to Professor Eugen Illenberger for inspiration and encouragement of this work.

[1]N. R. Council, *Database Needs for Modeling and Simulation of Plasma Processing* (National Academies Press, Washington, D.C., 1996).
[2]A. Chutjian, A. Garscadden, and J. M. Wadhera, Phys. Rep. **264**, 393 (1996).
[3]J. Rajput, L. Lammich, and L. H. Andersen, Phys. Rev. Lett. **100**, 153001 (2008).
[4]L. G. Christophorou and J. K. Olthoff, Int. J. Mass Spectrom. **205**, 27 (2001).
[5]I. Rozum, N. J. Mason, and J. Tennyson, J. Phys. B **36**, 2419 (2003).
[6]C. S. Trevisan, A. E. Orel, and T. N. Rescigno, Phys. Rev. A **72**, 062720 (2005).
[7]I. Rozum, N. J. Mason, and J. Tennyson, J. Phys. B **35**, 1583 (2002).
[8]I. Rozum, N. J. Mason, and J. Tennyson, New J. Phys. **5**, 155 (2003).
[9]I. Rozum, P. Limao-Vieira, S. Eden, J. Tennyson, and N. J. Mason, J. Phys. Chem. Ref. Data **35**, 267 (2006).
[10]K. Graupner, T. A. Field, and C. A. Mayhew, New J. Phys. **12**, 083035 (2010).
[11]T. M. Maddern, L. R. Hargreaves, J. R. Francis-Staite, M. J. Brunger, S. J. Buckman, C. Winstead, and V. McKoy, Phys. Rev. Lett. **100**, 063202 (2008).
[12]M.-T. Lee, I. Iga, L. E. Machado, L. M. Brescansin, E. A. Y Castro, and G. L. C. de Souza, Phys. Rev. A **74**, 052716 (2006).
[13]N. S. Shuman, T. M. Miller, J. F. Friedman, A. A. Viggiano, A. I. Maergoiz, and J. Troe, J. Chem. Phys. **135**, 054306 (2011).
[14]T. A. Field, A. E. Slattery, D. J. Adams, and D. D. Morrison, J. Phys. B **38**, 255 (2005).
[15]N. S. Shuman, T. M. Miller, C. M. Caples, and A. A. Viggiano, J. Phys. Chem. A **114**, 11100 (2010).
[16]N. S. Shuman, T. M. Miller, R. J. Bemish, and A. A. Viggiano, Phys. Rev. Lett. **106**, 018302 (2011).
[17]N. S. Shuman, T. M. Miller, N. Hizari, E. D. Luzik, and A. A. Viggiano, J. Chem. Phys. **133**, 234304 (2010).
[18]N. S. Shuman, T. M. Miller, A. A. Viggiano, E. D. Luzik, and N. Hizari, J. Chem. Phys. **134**, 044323 (2011).
[19]N. S. Shuman, T. M. Miller, A. A. Viggiano, and J. Troe, Int. J. Mass Spectrom. **306**, 123 (2011).
[20]T. M. Miller, Adv. At., Mol., Opt. Phys. **51**, 299 (2005).
[21]N. G. Adams and D. Smith, "Rate coefficients in astrochemistry: Laboratory studies of dissociative recombination and mutual neutralization and their relevance to intersteller chemistry," in *Rate Coefficients in Astrochemistry* (Kluwer Academic, The Netherlands, 1988), p. 173.
[22]T. M. Miller, J. F. Friedman, A. E. S. Miller, and J. F. Paulson, Int. J. Mass Spectrom. Ion Process. **149/150**, 111 (1995).
[23]J. H. D. Eland and J. Berkowitz, J. Chem. Phys. **67**, 5034 (1977).
[24]R. A. A. Boschi and D. R. Salahub, Can. J. Chem. **52**, 1217 (1974).
[25]*NIST Chemistry WebBook, NIST Standard Reference Database Number 69 (online, available:* http://webbook.nist.gov *2006-2008)*, edited by P. G. Linstrom and W. G. Mallard (National Institute of Standards and Technology, Gaithersburg, MD, 2005).
[26]T. Hsieh and R. J. Hanrahan, Int. J. Mass Spectrom. Ion Phys. **23**, 201 (1977).
[27]I. P. Fisher, J. B. Homer, and F. P. Lossing, J. Am. Chem. Soc. **87**, 957 (1965).
[28]J. Langer, S. Matejcik, and E. Illenberger, Phys. Chem. Chem. Phys. **4**, 5105 (2002).
[29]J. Langer, S. Matejcik, and E. Illenberger, Int. J. Mass Spectrom. **220**, 211 (2002).
[30]T. M. Miller, A. E. S. Miller, J. F. Paulson, and X. Liu, J. Chem. Phys. **100**, 8841 (1994).
[31]D. Smith and P. Spanel, Adv. At., Mol., Opt. Phys. **32**, 307 (1994).
[32]E. I. Dashevskaya, I. Litvin, E. E. Nikitin, and J. Troe, Phys. Chem. Chem. Phys. **10**, 1270 (2008).
[33]E. I. Dashevskaya, I. Litvin, E. E. Nikitin, and J. Troe, J. Phys. Chem. A **115**, 6825 (2011).
[34]T. Sunagawa, and H. Shimamori, in *International Symposium on Electron-Molecule Collisions and Swarms, Tokyo*, edited by Y. Hatano, H. Tanaka, and N. Kouchi (Institute of Technology, Tokyo, 1999).
[35]J. Troe, T. M. Miller, and A. A. Viggiano, J. Chem. Phys. **127**, 244304 (2007).
[36]J. Troe, T. M. Miller, and A. A. Viggiano, J. Chem. Phys. **127**, 244303 (2007).
[37]A. A. Viggiano, T. M. Miller, J. F. Friedman, and J. Troe, J. Chem. Phys. **127**, 244305 (2007).
[38]Y. Ikezoe, S. Matsuoka, M. Takebe, and A. Viggiano, *Gas Phase Ion-Molecule Reaction Rate Constants through 1986* (Maruzen, Tokyo, Japan, 1987).
[39]N. S. Shuman, T. M. Miller, J. F. Friedman, A. A. Viggiano, S. Maeda, and K. Morokuma, J. Chem. Phys. **135**, 024204 (2011).
[40]K. Graupner, T. A. Field, and L. Feketeova, New J. Phys. **8**, 314 (2006).
[41]A. Schramm, J. M. Weber, J. Kreil, D. Klar, M. W. Ruf, and H. Hotop, Phys. Rev. Lett. **81**, 778 (1998).
[42]S. Barsotti, M.-W. Ruf, and H. Hotop, Phys. Rev. Lett. **89**, 083201 (2002).
[43]J. Troe and V. G. Ushakov, J. Phys. Chem. A **110**, 6732 (2006).
[44]W. R. Stevens, B. Sztaray, N. S. Shuman, T. Baer, and J. Troe, J. Phys. Chem. A **113**, 573 (2008).
[45]J. Troe, Z. Phys. Chem. **223**, 347 (2009).
[46]R. V. Serauskas and E. W. Schlag, J. Chem. Phys. **42**, 3009 (1965).
[47]L. A. Curtiss, K. Raghavachari, P. C. Redfern, V. Rassolov, and J. A. Pople, J. Chem. Phys. **109**, 7764 (1998).
[48]I. I. Fabrikant and H. Hotop, J. Chem. Phys. **128**, 124308 (2008).
[49]D. Smith, P. Spanel, S. Matejcik, A. Stamatovic, T. D. Maerk, T. Jaffke, and E. Illenberger, Chem. Phys. Lett. **240**, 481 (1995).